

Poincaré Map Method for Limit Cycles in a Max-Plus Dynamical System

Shousuke Ohmori^{*}) and Yoshihiro Yamazaki

Faculty of Science and Engineering, Waseda University, Shinjuku, Tokyo 169-8555, Japan

**corresponding author: 42261timemachine@ruri.waseda.jp*

Abstract

Dynamical properties of limit cycles in a two-dimensional max-plus dynamical system are discussed. We apply a Poincaré map method to the limit cycles in order to reveal their stabilities. This method reduces the two dimensional system to a one-dimensional piecewise linear discrete dynamical system composed of the Poincaré map and its cross section. Basins for one of the limit cycles are derived by considering the inverse system of the original model. It is found that the obtained basins show a hierarchic structure. Relationship between the Poincaré map method and the method of piecewise linear mapping studied in integrable system theory for the limit cycles is discussed.

1 Introduction

An ultradiscrete equation is a difference equation with max-plus algebra. It can be derived from a difference equation by means of ultradiscretization[1]. This method converts a difference equation into ultradiscretized one by the following two procedures; (i) a positive variable in a difference equation, say x_n , is transformed into X_n by $x_n = \exp(X_n/\varepsilon)$, where ε is a positive parameter, and (ii) the ultradiscrete limits

$$\begin{cases} \lim_{\varepsilon \rightarrow +0} \varepsilon \log(e^{A/\varepsilon} + e^{B/\varepsilon} + \dots) = \max(A, B, \dots), \\ \lim_{\varepsilon \rightarrow +0} \varepsilon \log(e^{A/\varepsilon} \cdot e^{B/\varepsilon} \cdot \dots) = A + B + \dots, \end{cases} \quad (1)$$

are imposed. The ultradiscretization method has been successfully applied to integrable systems[2, 3]. One typical example is ultradiscrete Burgers equation[4].

The ultradiscretization method has also been applied to non-equilibrium dissipative systems such as reaction-diffusion systems [5, 6, 7, 8, 9, 10, 11, 12, 13]. Especially, we have focused on application to dynamical systems[10, 11, 12]. In general, ultradiscrete equations are composed of piecewise linear difference equations, and their dynamical properties, e.g., existence of fixed points and their stabilities, can be characterized as discrete dynamical system. In our studies, the dynamical properties of the ultradiscrete equations that exhibit bifurcations, namely, ultradiscrete bifurcations, have been discussed.

Here, we consider the following set of max-plus equations [11, 12]:

$$X_{n+1} = Y_n + \max(0, 2X_n), \quad (2)$$

$$Y_{n+1} = B - \max(0, 2X_n). \quad (3)$$

These equations are obtained from Sel'kov model via tropical discretization and ultradiscretization. We found that this model has the two different limit cycles, i.e., periodic solutions around an unstable fixed point. These limit cycles possess the following characteristic dynamical properties; (i) they are composed of seven states. (ii) any initial states without the unstable fixed point converges to one of the two limit cycles with finite iteration time steps.

In this paper, dynamical properties of these limit cycles are analytically discussed. By using Poincaré map, we rigorously characterize difference between the two limit cycles. In the next section, we review the dynamical properties of eqs.(2)-(3) with $B > 0$. By introducing a Poincaré section for the limit cycles and its Poincaré map, stabilities of these cycles are revealed in Sec.3. In Sec. 4, basins for one of the limit cycles are clarified. The discussion and the conclusion are given in Sec. 5 and 6, respectively.

2 Review for the limit cycles obtained from Eqs. (2)-(3)

To investigate the dynamical properties of eqs.(2)-(3), it is convenient to consider the two regions in $X_n Y_n$ -plane: I $\{(X_n, Y_n); X_n > 0\}$ and II $\{(X_n, Y_n); X_n \leq 0\}$. Equations (2)-(3) can be rewritten by the following matrix form:

$$\begin{pmatrix} X_{n+1} \\ Y_{n+1} \end{pmatrix} = \mathbf{A} \begin{pmatrix} X_n \\ Y_n \end{pmatrix} + \begin{pmatrix} 0 \\ B \end{pmatrix}, \quad (4)$$

where

$$\mathbf{A} = \begin{cases} \mathbf{A}_I = \begin{pmatrix} 2 & 1 \\ -2 & 0 \end{pmatrix} & \text{when } (X_n, Y_n) \text{ is in region I,} \\ \mathbf{A}_{II} = \begin{pmatrix} 0 & 1 \\ 0 & 0 \end{pmatrix} & \text{when } (X_n, Y_n) \text{ is in region II.} \end{cases} \quad (5)$$

From \mathbf{A}_I , it is found that the solution trajectory becomes a clockwise spiral moving away from the unstable fixed point $(B, -B)$. For \mathbf{A}_{II} , (B, B) is a stable fixed point and any $\mathbf{x}_0 = (X_0, Y_0)$ in region II has the subsequent trajectory composed of the three points $\{\mathbf{x}_0 = (X_0, Y_0), \mathbf{x}_1 = (Y_0, B), \mathbf{x}_2 = (B, B)\}$.

Hereafter we set $B > 0$. Note that both $(B, \pm B)$ are in region I. Previously we found the two clockwise periodic solutions \mathcal{C} and \mathcal{C}_s [12]; each of them is composed of the seven points shown in Table 1 and Fig. 1. We have also numerically shown that \mathcal{C} and \mathcal{C}_s are limit cycles. In the next section, we prove this fact rigorously by means of a Poincaré map defined on a Poincaré section for the limit cycles.

Table 1: The seven states in limit cycles \mathcal{C} and \mathcal{C}_s . We denote these seven points in \mathcal{C} and \mathcal{C}_s as $\{\mathbf{x}_j^{\mathcal{C}}\}$ and $\{\mathbf{x}_j^{\mathcal{C}_s}\}$, respectively, where $j = 0, \dots, 6$.

	\mathcal{C}	\mathcal{C}_s
\mathbf{x}_0	(B, B)	$(\frac{B}{15}, B)$
\mathbf{x}_1	$(3B, -B)$	$(\frac{17B}{15}, \frac{13B}{15})$
\mathbf{x}_2	$(5B, -5B)$	$(\frac{47B}{15}, -\frac{19B}{15})$
\mathbf{x}_3	$(5B, -9B)$	$(5B, -\frac{79B}{15})$
\mathbf{x}_4	$(B, -9B)$	$(\frac{71B}{15}, -9B)$
\mathbf{x}_5	$(-7B, -B)$	$(\frac{7B}{15}, -\frac{127B}{15})$
\mathbf{x}_6	$(-B, B)$	$(-\frac{113B}{15}, \frac{B}{15})$

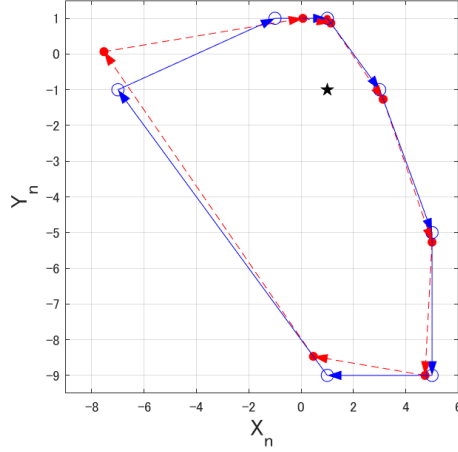


Figure 1: The trajectories of \mathcal{C} (open circles) and \mathcal{C}_s (solid circles) for $B = 1$ [12]. The black star shows $(B, -B) = (1, -1)$.

3 Dynamical properties of \mathcal{C} and \mathcal{C}_s

Equation (4) shows that a point in region I moves away from the fixed point clockwise, i.e., the fixed point becomes an unstable focus, and reaches region II after some iteration steps. When $\mathbf{x}_0 = (X_0, Y_0)$ belongs to region II, then $\mathbf{x}_1 = (Y_0, B)$. Therefore, every trajectory must pass a line $L_B \equiv \{\mathbf{x}_n = (X_n, B), X_n \in (0, \infty)\}$. In particular, $\mathbf{x}_0^{\mathcal{C}}$ and $\mathbf{x}_0^{\mathcal{C}_s}$ in Table I return to themselves on L_B as shown in Fig. 2. Therefore, L_B can be regarded as Poincaré section for \mathcal{C} and \mathcal{C}_s . Next, we focus on trajectories starting at a point on L_B and construct a Poincaré map.

3.1 Construction of the Poincaré Map

Set $\mathbf{x}_0 = (X_0, B)$ on L_B , where $X_0 > 0$. Based on eq.(4) with $\mathbf{A} = \mathbf{A}_I$, the trajectory starting from \mathbf{x}_0 becomes as follows:

$$\begin{aligned}
 \{\mathbf{x}_0 &= (X_0, B) \rightarrow \mathbf{x}_1 = (2X_0 + B, -2X_0 + B) \rightarrow \mathbf{x}_2 = (2X_0 + 3B, -4X_0 - B) \\
 \rightarrow \mathbf{x}_3 &= (5B, -4X_0 - 5B) \rightarrow \mathbf{x}_4 = (-4X_0 + 5B, -9B) \rightarrow \mathbf{x}_5 = (-8X_0 + B, 8X_0 - 9B) \\
 \rightarrow \mathbf{x}_6 &= (-8X_0 - 7B, 16X_0 - B) \rightarrow \mathbf{x}_7 = (-B + 16X_0, B) \rightarrow \dots\}.
 \end{aligned} \tag{6}$$

To obtain the first return points for the trajectory for eq.(4) on L_B , which allow us the construction of Poincaré map, we consider the following cases depending on the sign of x -component of

$\mathbf{x}_4 \sim \mathbf{x}_7$ in (6).

Case 1. When $\frac{5B}{4} \leq X_0$, \mathbf{x}_4 is in region II-1, $X_0 \leq 0, Y_0 \leq 0$. Then $\mathbf{x}_0 = (X_0, B)$ reaches

$$\mathbf{x}_0^c = (B, B) \text{ with six iteration step.}$$

Case 2. When $\frac{9B}{8} < X_0 < \frac{5B}{4}$, $\mathbf{x}_0 \sim \mathbf{x}_4$ in region I, \mathbf{x}_5 is in region II-2, $X_0 \leq 0, Y_0 > 0$, since

$$-8X_0 + B < 0 \text{ and } 0 < 8X_0 - 9B. \text{ Then, } \mathbf{x}_6 = (8X_0 - 9B, B) \text{ becomes on } L_B \text{ where}$$

$$0 < 8X_0 - 9B < B.$$

Case 3. When $\frac{B}{8} < X_0 \leq \frac{9B}{8}$, \mathbf{x}_5 is in region II-1, since $-8X_0 + B < 0$ and $8X_0 - 9B \leq 0$.

Then $\mathbf{x}_0 = (X_0, B)$ reaches \mathbf{x}_0^c with seven iteration steps.

Case 4. When $\frac{B}{16} < X_0 < \frac{B}{8}$, $\mathbf{x}_0 \sim \mathbf{x}_5$ in region I. \mathbf{x}_6 is in region II-2, since $16X_0 - B > 0$.

Then we have $\mathbf{x}_7 = (-B + 16X_0, B)$ where $0 < -B + 16X_0 < B$ on L_B .

Case 5. When $X_0 \leq \frac{B}{16}$, \mathbf{x}_6 is in region II-1, and hence $\mathbf{x}_0 = (X_0, B)$ reaches \mathbf{x}_0^c with eight

iteration steps.

By considering these cases, we can construct Poincaré map, which is an iteration map, $P :$

$(0, \infty) \rightarrow (0, B]$, as follows;

$$P(X_0) = \begin{cases} B & (0 < X_0 \leq \frac{B}{16}) \\ 16X_0 - B & (\frac{B}{16} < X_0 < \frac{B}{8}) \\ B & (\frac{B}{8} \leq X_0 \leq \frac{9B}{8}) \\ 8X_0 - 9B & (\frac{9B}{8} < X_0 < \frac{5B}{4}) \\ B & (\frac{5B}{4} \leq X_0). \end{cases} \quad (7)$$

In general, the discrete dynamical system composed of Poincaré map and its section can characterize dynamical properties of periodic solutions such as \mathcal{C} and \mathcal{C}_s [14, 15].

3.2 Graphical analysis of $(P, (0, \infty))$

We investigate the dynamical properties of P in detail. Equation (7) forms a one-dimensional piecewise linear discrete dynamical system. This dynamical properties can be easily grasped

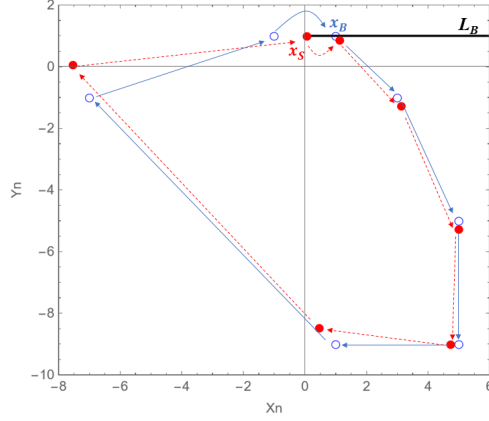


Figure 2: Definition of the Poincaré section L_B for \mathcal{C} (open circle) and \mathcal{C}_s (filled circle) with $B = 1$.

by using the graphical analysis[15]. Figure 3 shows the graph of $X_{n+1} = P(X_n)$. The graph intersects the diagonal $X_{n+1} = X_n$ at two points $X_n = X_s \equiv \frac{B}{15}$ and $X_n = B$, which are fixed points. These dynamical properties obtained by graphical analysis can be summarized as follows;

(i) When $0 < X_0 \leq \frac{B}{16}$, $\frac{B}{8} \leq X_0 \leq \frac{9B}{8}$, or $\frac{5B}{4} \leq X_0$, $P(X_0) = B$.

(ii) When $\frac{B}{16} < X_0 < X_s$ ($X_s < X_0 < \frac{B}{8}$), there exists an iteration step m , where $0 < P^m(X_0) \leq$

$$\frac{B}{16} \left(\frac{B}{8} \leq P^m(X_0) < B \right) \text{ and } P^{m+1}(X_0) = B.$$

(iii) When $\frac{9B}{16} < X_0 < \frac{5B}{4}$, $0 < P(X_0) = 8X_0 - 9B < B$. Especially when $X_0 = X'_s \equiv \frac{17B}{15}$,

$$P(X'_s) = X_s \text{ otherwise there exists } m \text{ where } P^m(X_0) = B.$$

Note that $X = B$ is a stable fixed point, whereas $X = X_s$ is an unstable fixed point. Therefore, we can conclude that \mathcal{C} is a stable limit cycle and \mathcal{C}_s is an unstable one.

4 Basins of \mathcal{C}_s

In the previous section, we show that \mathcal{C}_s is the unstable limit cycle. However, the property (iii) suggests that there are some regions in $X_n Y_n$ -plane whose points converge to \mathcal{C}_s . Here, we find such regions, namely, basins of \mathcal{C}_s .

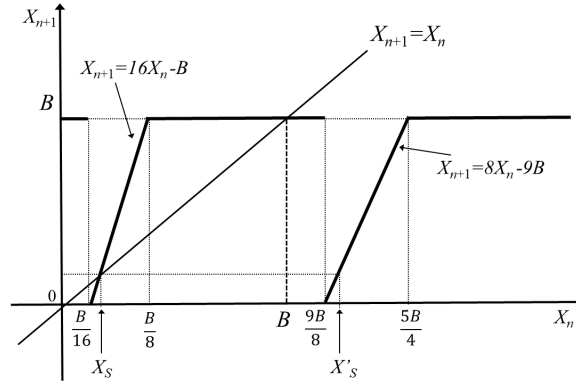


Figure 3: The graphs of the Poincaré map $P(X)$, eq.(7).

4.1 Basins in region II

As shown in the previous section, only two points $\mathbf{x}_s = (\frac{B}{15}, B)$ and $\mathbf{x}'_s = (\frac{17B}{15}, B)$ on L_B reach \mathcal{C}_s . Then, we can find the following two basins \mathcal{B}_0 and \mathcal{B}'_0 in region II-2, shown in Fig. 4, whose points arrive at \mathbf{x}_s or \mathbf{x}'_s with next iteration step:

$$\mathcal{B}_0 = \{(X_0, \frac{B}{15}); X_0 \leq 0\}, \quad \mathcal{B}'_0 = \{(X_0, \frac{17B}{15}); X_0 \leq 0\}. \quad (8)$$

Note that there is no points in region II-1 which becomes a basin for \mathcal{C}_s .

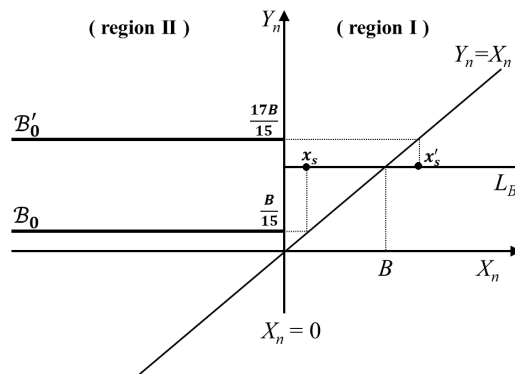


Figure 4: Basins of \mathcal{C}_s in region II.

4.2 Basins in region I

To elucidate basins of \mathcal{C}_s in region I, the following backward dynamical system for eq.(4) with $\mathbf{A} = \mathbf{A}_I$ is considered:

$$\begin{pmatrix} X_{n+1} \\ Y_{n+1} \end{pmatrix} = \mathbf{A}_I^{-1} \begin{pmatrix} X_n \\ Y_n \end{pmatrix} + \begin{pmatrix} \frac{B}{2} \\ -B \end{pmatrix}, \quad (9)$$

where $\mathbf{A}_I^{-1} = \begin{pmatrix} 0 & -\frac{1}{2} \\ 1 & 1 \end{pmatrix}$. We denote the backward trajectory of \mathbf{x}_0 obtained from eq.(9) as $\{\mathbf{x}_0, \mathbf{x}_1^{inv}, \mathbf{x}_2^{inv}, \mathbf{x}_3^{inv}, \dots\}$ ($= \{\mathbf{x}_n^{inv}\}$), hereafter. Clearly the relation

$$\mathbf{x}_{i+1}^{inv} = \mathbf{A}_I^{-1} \mathbf{x}_i^{inv} + \left(\frac{B}{2}, -B\right) \Leftrightarrow \mathbf{x}_i^{inv} = \mathbf{A}_I \mathbf{x}_{i+1}^{inv} + (0, B) \quad (10)$$

holds for $i = 0, 1, \dots$, ($\mathbf{x}_0^{inv} = \mathbf{x}_0$). If (X_0, Y_0) is in region I and its next iteration point is in \mathcal{B}'_0 , then $(X_1, \frac{17B}{15}) = \mathbf{A}_I(X_0, Y_0) + (0, B)$ is satisfied and we obtain $X_0 = -\frac{B}{15} < 0$. Focusing on the trajectory with a point in both region I and the basin of \mathcal{C}_s , any point in this trajectory of region II belongs only to \mathcal{B}_0 . Therefore, there is no point in region I whose trajectory has a point on \mathcal{B}'_0 .

Here we set the initial point \mathbf{x}_0 in \mathcal{B}_0 , namely $\mathbf{x}_0(z) = (z, \frac{B}{15})$, where $z \leq 0$. Based on eq.(9), $\mathbf{x}_0(z)$ becomes $\mathbf{x}_n^{inv}(z) = (X_n^{inv}(z), Y_n^{inv}(z))$, where

$$\begin{aligned} X_n^{inv}(z) &= B + 2^{-\frac{n}{2}} \left\{ \cos\left(\frac{\pi}{4}n\right)(z - B) - \sin\left(\frac{\pi}{4}n\right)\left(z + \frac{B}{15}\right) \right\}, \\ Y_n^{inv}(z) &= -2X_{n+1}^{inv}(z) + B. \end{aligned} \quad (11)$$

Now we consider a region of z in which $X_n^{inv}(z) > 0$. Note that the term $\left\{ \cos\left(\frac{\pi}{4}n\right)(z - B) - \sin\left(\frac{\pi}{4}n\right)\left(z + \frac{B}{15}\right) \right\}$ in eq.(11) has the same value for $n = \ell + 8m$ ($\ell = 1, 2, \dots, 8$, and $m = 0, 1, 2, \dots$).

When $\ell = 8$, $n = 8(m+1)$, eq.(11) becomes $X_n^{inv}(z) = 2^{-\frac{n}{2}}z + (1 - 2^{-\frac{n}{2}})B$. Then, $z > (1 - 2^{-\frac{n}{2}})B$ brings about $X_n^{inv}(z) > 0$. According to the relation $(1 - 2^{\frac{8m}{2}})B > (1 - 2^{\frac{8(m+1)}{2}})B$, we have

$X_n^{inv}(z) > 0$ for $n = 8m$ if $z > (1 - 2^{\frac{8}{2}})B = -15B$. Namely, whenever $z > -15B$, $\mathbf{x}_n^{inv}(z)$ always belongs to region I. Applying this consideration to $n = \ell + 8m$, $\ell = 1 \sim 7$, $m = 0, 1, 2, \dots$, the

sufficient conditions for z that $\mathbf{x}_n^{inv}(z)$ belongs to region I can be obtained as follows;

- (i) $z \leq 0$ for $n = \ell + 8m, \ell = 1 \sim 5,$
- (ii) $-\frac{121}{15}B \leq z \leq 0$ for $n = 6 + 8m,$
- (iii) $-\frac{113}{15}B \leq z \leq 0$ for $n = 7 + 8m,$
- (iv) $-15B < z \leq 0$ for $n = 8(m + 1).$

The condition (i) shows that $\mathbf{x}_1^{inv}(z)$ with $z \leq 0$ is in region I and reaches \mathcal{B}_0 with next iteration step by eq.(4). Therefore, $\mathcal{B}_1 = \{\mathbf{x}_1^{inv}(z), z \leq 0\}$ is a basin of \mathcal{C}_s in region I. Similarly, we can obtain the other basins in region I by considering (i) \sim (iv), as follows:

$$\mathcal{B}_n = \{\mathbf{x}_n^{inv}(z), z \leq 0\} \quad \text{for } n = 1 \sim 5, \quad (12)$$

$$\mathcal{B}_6 = \{\mathbf{x}_6^{inv}(z), -\frac{121B}{15} \leq z \leq 0\}, \quad (13)$$

$$\mathcal{B}_n = \{\mathbf{x}_n^{inv}(z), -\frac{113B}{15} \leq z \leq 0\} \quad \text{for } 7 \leq n. \quad (14)$$

It is noted that when \mathbf{x}_0 is in a basin \mathcal{B}_n , the trajectory $\{\mathbf{x}_n\}$ passes successively all basins \mathcal{B}_j with $j = n, n - 1, \dots, 1$, and finally reach \mathcal{B}_0 .

4.3 Properties of Basins

We comment some properties of the basins $\mathcal{B}_n, n = 0, 1, 2, \dots,$ and \mathcal{B}'_0 . (i) \mathcal{B}_6 and \mathcal{B}_5 include $\mathbf{x}_s = (\frac{B}{15}, B)$ and $\mathbf{x}'_s = (\frac{17B}{15}, B)$ on L_B , respectively. (ii) each $\mathbf{x}_j^{C_s}$ ($j = 1 \sim 6$) coincides with $\mathbf{x}_{6-j}^{inv}(-\frac{113B}{15})$ on \mathcal{B}_{6-j} . (iii) \mathbf{x}_0 in \mathcal{B}_n has the trajectory $\{\mathbf{x}_0, \mathbf{x}_1, \mathbf{x}_2, \dots, \mathbf{x}_n\}$, each \mathbf{x}_j passing successively \mathcal{B}_{n-j} with $j = 0 \sim n$, and then $\mathbf{x}_{n+1} = \mathbf{x}_s = \mathbf{x}_0^{C_s}$. (iv) For $n = 0, 1, 2, \dots,$ \mathcal{B}_n connects with \mathcal{B}_{n+7} as shown in Fig. 5. Indeed, the following relation holds:

$$\mathbf{x}_n^{inv}(0) = \mathbf{x}_{n+7}^{inv}(-\frac{113B}{15}) \quad \text{for } n = 0, 1, 2, \dots. \quad (15)$$

Also, we can show that \mathcal{B}'_0 connects \mathcal{B}_6 from the relation $\mathbf{x}_6^{inv}(-\frac{121B}{15}) = (0, \frac{17B}{15})$. It is found from Fig. 5 that the basins in region I are distributed around $(B, -B)$ spirally. This fact can be

confirmed from the following short consideration. First, the relation $\mathbf{x}_{n+1}^{inv}(z) = \mathbf{A}_I^{-1}\mathbf{x}_n^{inv}(z) + (\frac{B}{2}, -B)$ holds for any z by eq.(10). This relation shows that \mathcal{B}_{n+1} coincides with the image of \mathcal{B}_n by the linear mapping of eq.(9). Since eq.(9) is the inverse of eq.(4) with $\mathbf{A} = \mathbf{A}_I$, its dynamics is characterized as the anticlockwise spiral sink with the center $(B, -B)$. Thus, the basins are distributed spirally. Note that this property gives rise to the hierarchic and self-similar structure of basins as shown in Fig. 6.

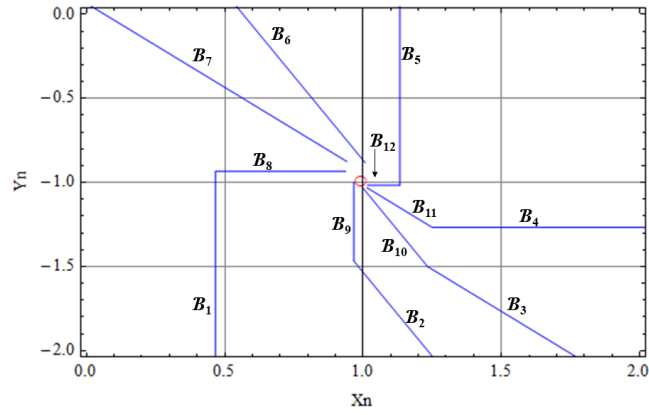


Figure 5: Basins $\mathcal{B}_1 \sim \mathcal{B}_{12}$. These are distributed around an unstable fixed point $(B, -B)$ depicted by red circle.

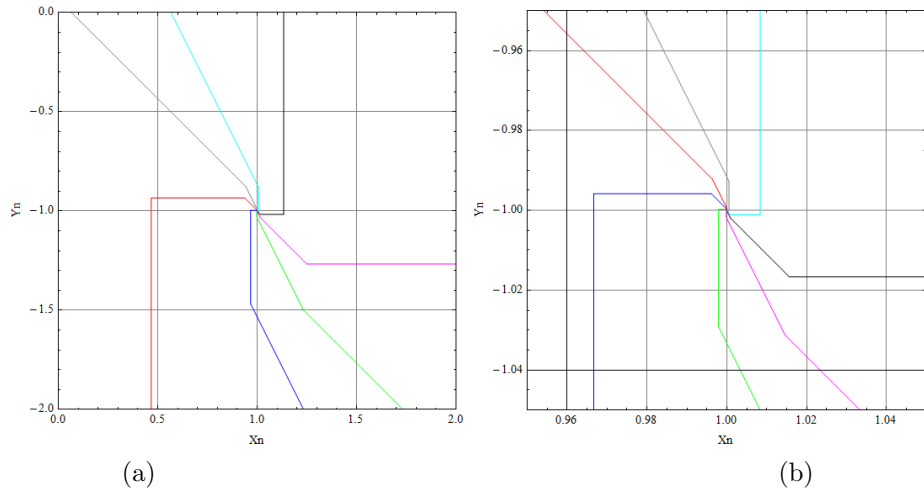


Figure 6: Self-similarity of basins in region I. Both figures show basins $\mathcal{B}_1 \sim \mathcal{B}_{50}$ with $B = 1$ in the region (a) $[0, 2] \times [-2, 0]$, (b) $[0.95, 1.05] \times [-1.05, -0.95]$. The basins' colors (red, blue, green, magenta, black, cyan, and gray) represent their connection; the basins which have the same color are connected each others.

5 Discussion

Here, we discuss the periodicity of \mathcal{C} and \mathcal{C}_s from a different point of view[16]. For simplicity, we set $B = 1$ in this section. From eqs.(2)-(3), we have a relation $X_{n+1} + Y_{n+1} = Y_n + 1$. Inserting this relation into eq.(3), we obtain the following piecewise linear mapping with only variable Y :

$$Y_{n+1} = 1 + \min(0, 2(Y_n - Y_{n-1} - 1)). \quad (16)$$

Equation (16) is composed of two mappings, $Y_{n+1} = 2Y_n - 2Y_{n-1} - 1$ when $Y_n \leq Y_{n-1} + 1$ and $Y_{n+1} = 1$ when $Y_n \geq Y_{n-1} + 1$. Here, we consider a heptagon Γ whose vertexes are given in xy -plane ($x = Y_{n-1}, y = Y_n$) as the following seven points, $\{(1, 1), (1, -1), (-1, -5), (-5, -9), (-9, -9), (-9, -1), (-8, 1)\}$. Figure 7 shows Γ . Note that each (x, y) on Γ satisfies the following equation:

$$\min(y - 2x + 3, y - x + 4, y + 9, x + 9, -y + 2x + 17, -y + 1, -x + 1) = 0. \quad (17)$$

It is noted that the point $(-1, 1)$ and the vertexes of Γ without $(-8, 1)$ compose of a clockwise periodic solution \mathcal{C}^Γ of eq.(16), which is shown in Fig. 7 as the blue filled circles. $(-8, 1)$ is the point mapped by eq.(16) from the point $(-9, -8)$, which is an intersection between Γ and $Y_n = Y_{n-1} + 1$. The polygon generated from a piecewise linear mapping, Γ in this case, has been widely studied in the context of ultradiscretization for the integrable systems[2, 17]. In the following, we apply to Γ the method used in ultradiscretizing the Quispel-Robert-Thompson system[17].

We focus on a half-open line segment from $(1, 1)$ to $(1, -1)$ in Γ , say $S \equiv \{(1, y), -1 \leq y < 1\}$. All points on S return to S by eq.(16) after a certain iteration step. Here, we divide S into the following three subsegments $R_0 = \{(x, y) \in S, |(1, 1) - (x, y)| \leq \frac{1}{16}\}$, $B_0 = \{(x, y) \in S, \frac{1}{16} < |(1, 1) - (x, y)| < \frac{1}{8}\}$, and $G_0 = \{(x, y) \in S, \frac{1}{8} \leq |(1, 1) - (x, y)| \leq 1\}$ in the ratio of 1 : 1 : 14. Recall that eq.(16) behaves as different linear mappings in the regions $Y_n \leq Y_{n-1} + 1$ and

$Y_n \geq Y_{n-1} + 1$, and hence the internal ratio for each segment is retained. By using this fact, each segment composing of Γ can be divided into the three subsegments corresponding to R_0, B_0 , and G_0 . Figure 8 (a) and (b) show the divisions of S and of each segment, respectively. As shown in Fig. 8 (b), the trajectories starting from the three subsegments of S by eq.(16) are given as follows:

$$\begin{aligned}
R_0 &\rightarrow R_1 \rightarrow \cdots \rightarrow R_6 \rightarrow (1, -1) \\
B_0 &\rightarrow B_1 \rightarrow \cdots \rightarrow B_6 \rightarrow S \\
G_0 &\rightarrow G_1 \rightarrow \cdots \rightarrow G_5 \rightarrow (1, -1).
\end{aligned} \tag{18}$$

From these trajectories, we find that the only subsegment B_0 is stretched over the whole segment S whereas R_0 and G_0 converge to \mathcal{C}^Γ after a round of mapping by eq.(16).

In order to characterize the self-similar structure of S , let us introduce an internally dividing point r_k defined by

$$r_k = \frac{\text{length from } (1, 1) \text{ to } Q_k}{\text{length of } S} = \frac{|1 - q_k|}{2} \tag{19}$$

where $Q_k = (1, q_k)$ denotes a point on S at the k -th return from an initial point $Q_0 = (1, q_0)$ on S . From the trajectories (18) for R_0, B_0 , and G_0 , r_k satisfies the following recurrence formula:

$$r_{k+1} = \begin{cases} 1 & (0 < r_k \leq \frac{1}{16}), \\ 16r_k - 1 & (\frac{1}{16} < r_k < \frac{1}{8}), \\ 1 & (\frac{1}{8} \leq r_k \leq 1). \end{cases} \tag{20}$$

r_k has just two fixed points $r_k = 1$ and $r_k = \frac{1}{15}$ corresponding to $Q_k = (1, -1)$ and $Q_k = (\bar{x}, \bar{y}) \equiv (1, \frac{13}{15})$ on S , respectively. Stretching B_0 to S is identified with the iteration $r_k \rightarrow r_{k+1} = 16r_k - 1$ for $\frac{1}{16} < r_k < \frac{1}{8}$ (Fig. 8 (a)), and by making use of the graphical analysis as well as Fig. 3, we can confirm that as $k \rightarrow \infty$ all point on S without the fixed point (\bar{x}, \bar{y}) is absorbed to \mathcal{C}^Γ . In other words, only the point (\bar{x}, \bar{y}) does not converge to \mathcal{C}^Γ but returns to itself by any iteration step of $r_k \rightarrow r_{k+1}$. Therefore, the trajectory starting from (\bar{x}, \bar{y}) by eq.(16) constructs a cycle

with seven points on Γ , say \mathcal{C}_s^Γ , which is different from \mathcal{C}^Γ . Note that \mathcal{C}^Γ is stable and \mathcal{C}_s^Γ is unstable since B_0 is stretched onto S .

Equation (20) coincides with the form of the Poincaré map (7) for $B = 1$ whose domain is restricted in $(0, 1]$. Actually, the mapping $r_k \rightarrow r_{k+1}$ can be associated with P as follows. Let us introduce a mapping $h : (x, y) \mapsto (X_n, Y_n) = (1 - y + x, y)$ by which xy -plane can be transformed homeomorphically onto $X_n Y_n$ -plane. Then, eq.(16) becomes topologically conjugate to the system of eqs.(2)-(3) relative to h . Then, \mathcal{C}^Γ , S , and \mathcal{C}_s^Γ transform the limit cycle \mathcal{C} , the segment I from \mathbf{x}_0^C to \mathbf{x}_1^C , and \mathcal{C}_s , respectively, where \mathbf{x}_0^C and \mathbf{x}_1^C are the points composing of \mathcal{C} stated in Table 1 of Sec. 2. In $X_n Y_n$ -plane, we set a point $(x_0, 1)$ with $0 < x_0 < 1$ on L_B ($B = 1$). Then $(x_0, 1)$ maps to $(1, -2x_0 + 1)$ on S in xy -plane. Taking $(1, -2x_0 + 1)$ as the initial point on S , we obtain from eq.(19)

$$r_0 = \frac{|1 - (-2x_0 + 1)|}{2} = x_0. \quad (21)$$

When we set $x_0 = 1$, $(x_0, 1) = (1, 1)$ on L_B maps to $(1, -1)$ on S and we obtain $r_0 = 1 = x_0$. Therefore, the value of an internally dividing point r_0 is equal to the value x_0 on the Poincaré subsection $(0, 1]$ and the mapping $r_k \rightarrow r_{k+1}$ completely corresponds to the Poincaré map $x_{k+1} = P(x_k)$, restricted on $0 < x_k \leq 1$. Note that the stability of \mathcal{C} and \mathcal{C}_s analyzed by the Poincaré map $x_{k+1} = P(x_k)$ can be also understood through the mapping $r_k \rightarrow r_{k+1}$ characterizing the self-similar structure of S in xy -plane. We expect that the method developed from the piecewise linear mapping in the integrable system theory can be further applied to the study of periodic structures found in generally (non-integrable) max-plus dynamical systems.

6 Conclusion

Dynamical properties of the limit cycles \mathcal{C} and \mathcal{C}_s found in the max-plus model (eqs.(2)-(3)) are investigated. With the aid of Poincaré map method, we confirm their stability; \mathcal{C} is stable

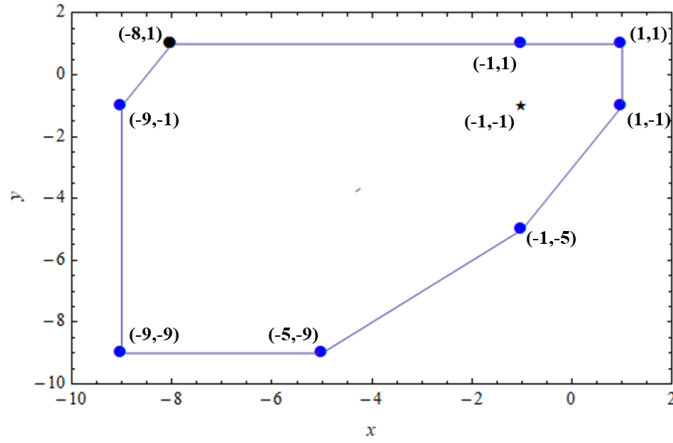


Figure 7: The heptagon Γ in xy -plane. The blue solid points provide \mathcal{C}^Γ .

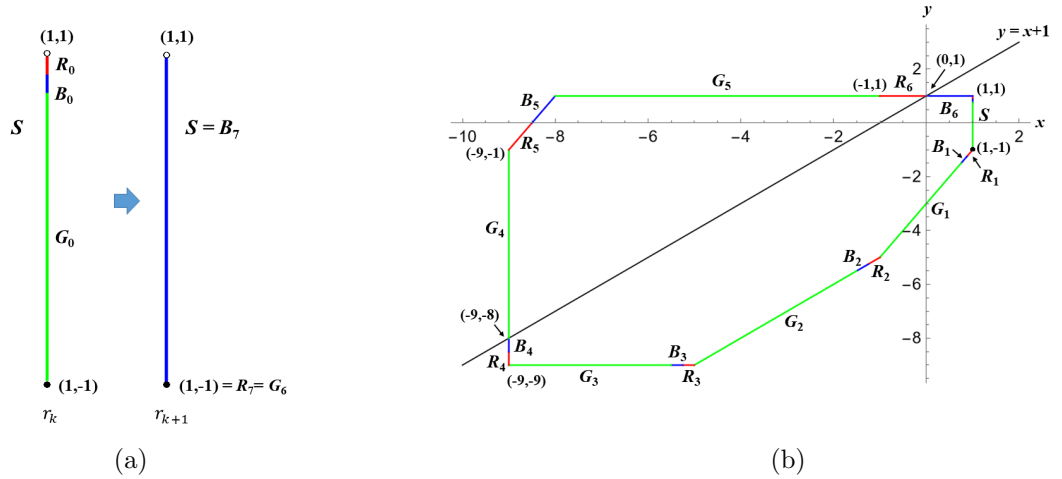


Figure 8: The sketches of the divisions of (a) S and (b) each segment. Equation (16) maps the three subsegments R_0 , B_0 , and G_0 of S as follows: $R_0 \rightarrow R_1 \rightarrow \dots \rightarrow R_6 \rightarrow R_7 = (1, -1)$, $B_0 \rightarrow B_1 \rightarrow \dots \rightarrow B_6 \rightarrow B_7 = S$, $G_0 \rightarrow G_1 \rightarrow \dots \rightarrow G_5 \rightarrow G_6 = (1, -1)$.

and \mathcal{C}_s is unstable. For \mathcal{C}_s , we identify its basins \mathcal{B}_n , $n = 0, 1, 2, \dots$, and \mathcal{B}'_0 . These basins are distributed around the unstable fixed point and have a hierarchic and self-similar structure. We apply the method of piecewise linear mapping studied in ultradiscretizing the Quispel-Robert-Thompson system to our max-plus system and reveal the connection of the mapping of the internally dividing point with the Poincaré map method.

Acknowledgement

The authors are grateful to Prof. D. Takahashi, Prof. T. Yamamoto, and Prof. Emeritus

A. Kitada at Waseda University for useful comments and encouragements. This work was supported by Sumitomo Foundation, Grant Number 200146.

References

- [1] T. Tokihiro, D. Takahashi, J. Matsukidaira, and J. Satsuma, *Phys. Rev. Lett.* **76**, 3247 (1996).
- [2] B. Grammaticos, Y. Ohta, A. Ramani, D. Takahashi, and K. M. Tamizhmani, *Phys. Lett. A* **226**, 53 (1997).
- [3] D. Takahashi, T. Tokihiro, B. Grammaticos, Y. Ohta, and A. Ramani, *J. Phys. A:Math. Gen.* **30** 7953 (1997)
- [4] K. Nishinari and D. Takahashi, *J. Phys. A: Math. Gen.* **31** 5439 (1998).
- [5] M. Murata, *J. Differ. Equations Appl.* **19** 1008 (2013).
- [6] S. Ohmori and Y. Yamazaki, *Prog. Theor. Exp. Phys.* 083A01 (2014).
- [7] K. Matsuya and M. Murata, *Discrete Contin. Dyn. Syst. B* **20** 173 (2015).
- [8] M. Murata, *J. Phys. A Math, Theor.* **48** 255202 (2015).
- [9] S. Ohmori and Y. Yamazaki, *J. Phys. Soc. Jpn.* **85** 045001 (2016).
- [10] S. Ohmori and Y. Yamazaki, *J. Math. Phys.* **61** 122702 (2020).
- [11] Y. Yamazaki and S. Ohmori, *J. Phys. Scr. Jpn.* **90** 103001 (2021).
- [12] S. Ohmori and Y. Yamazaki, arXiv:2103.16777v1.
- [13] S. Isojima and S. Suzuki, *Nonlinearity.* **35** 1468 (2022).

- [14] J. Guckenheimer and P. Holmes, *Nonlinear Oscillations, Dynamical Systems, and Bifurcations of Vector Fields* (Springer, New York, 1983).
- [15] C. Robinson, *Dynamical systems -Stability, Symbolic Dynamics, and Chaos-, 2ed edition* (CRC Press, Florida 1999).
- [16] D. Takahashi, private communication.
- [17] D. Takahashi and M. Iwao, *Bilinear Integrable Systems: from Classical to Quantum, Continuous to Discrete* (Springer, 2002) pp.291-300.